Ground-Motion Data from Seismicity Induced in the Southern Montney Formation, Northeastern British Columbia

A.M.M. Bustin, The University of British Columbia, Vancouver, BC, abustin@eos.ubc.ca

E.O. Munson, The University of British Columbia, Vancouver, BC

D.J. Jones, The University of British Columbia, Vancouver, BC

G.R.L. Chalmers, The University of British Columbia, Vancouver, BC

Bustin, A.M.M., Munson, E.O., Jones, D.J. and Chalmers, G.R.L. (2019): Ground-motion data from seismicity induced in the southern Montney Formation, northeastern British Columbia; *in* Geoscience BC Summary of Activities 2018: Energy and Water, Geoscience BC, Report 2019-2, p. 55–62.

Introduction

The limited availability of data to researchers is arguably the greatest challenge to advancement of the understanding of induced seismicity in Western Canada and hence to the development of proactive mitigation schemes and frameworks for hazard assessment. To address the data gap, a 15-station array is being developed to densely monitor hydraulic-fracturing operations in the Montney Formation. The pre-existing accelerographs, which are now providing real-time data to an online interactive platform, were deployed to monitor two disposal wells and four hydraulic-fracturing operations in the past year. Although no events have yet been detected after 1.5 years by the station installed to monitor a disposal in a seismically inactive area, 12 events were recorded on the four-station array installed to monitor a disposal in an active area. Single stations were deployed within 3 km of the four completions, three of which were in seismically active areas. No events were detected on the smallest of the three operations, while four and six events were recorded during the two larger operations. In total, 25 events were recorded during the deployments, with site-corrected, peak ground accelerations (PGAs) ranging from 0.027%g to 0.23%g. The real-time ground-motion parameters are calculated for the geometric mean of the horizontal components, which are then corrected to a reference site using correction factors calculated during post-processing. For events located by the NRCan network or the local operator-deployed array, the corrected PGAs were plotted versus hypocentral distances. A good fit between the data and the prediction models was demonstrated by Babaie Mahani and Kao (2017). The dataset was also used to confirm the completeness threshold.

In order to detect smaller events and to facilitate locating events and calculating magnitudes in real time, one of the stations was upgraded to include a three-component (3C), 4.5 Hz geophone. This paired station was recently deployed to a seismically active area, where it is co-located with a long-term station and two temporary stations. The four accelerometers were installed at different depths (30, 60, 90 and 120 cm) in order to test the impact of burial depth on the response spectra. Additional ongoing work includes the addition of algorithms to the online portal for real-time calculation of hypocentres and magnitudes. Following testing of the paired station, geophones will be added to the other stations and the entire array will be deployed to densely monitor hydraulic-fracturing operations on three to five multilateral wellpads. The datasets will then be integrated into three-dimensional (3-D) hydro-geomechanical models to address the study's objectives, summarized by Bustin and Longobardi (2017).

This publication is also available, free of charge, as colour digital files in Adobe Acrobat® PDF format from the Geoscience BC website: http://www.geosciencebc.com/s/SummaryofActivities.asp.

Station Design

The design for this low-cost, mobile, easy-to-install station was modified from the early earthquake detectors developed by the Earthquake Engineering Research Facility (EERF) at The University of British Columbia and installed in BC schools for the Earthquake Early Warning System (Azpiri, 2016). The units are powered by a solar panel with an absorbent glass mat (AGM) deep-cycle battery. For long-term and distant stations, two solar panels and three batteries were used for backup. Advanced RISC (reduced instruction set computer) machine (ARM) processors running Linux, which are stored within protective (weather- and animal-proof) cases, run the system, while the data are stored on ultra–high-capacity USB drives. The protective case also encloses a global positioning system (GPS) for timing and station location. Telemetry is currently provided by cellphone modems with antennas and, in some cases, machine-to-machine (M2M) cellphone boosters to improve the signal. Satellite M2M systems are currently being investigated to provide telemetry in more remote locations. The solar panels are mounted on an aluminum frame that was designed in house, which has recently been upgraded to include a raised, covered shelf to enclose the protective case and batteries off the ground.

The commercial, 3C, microelectromechanical systems (MEMS) accelerometers are enclosed in sealed tubes, 50–80 cm in length and 7.5 cm in diameter, that are buried beneath surficial alluvium with a shovel to depths of 30–120 cm. To improve the detection, location and magnitude calculation of events, the stations are being augmented with commercial, 3C, 4.5 Hz geophones. The geophones are shallowly buried in conical, 15 cm long enclosures. The first of these paired stations was recently deployed for testing.

The raw data are collected and stored at 250 Hz for the accelerometers and 500 Hz for the geophones. When a ground motion is recorded above a set threshold, an alert is emailed and the data are transferred to the online, interactive platform (dashboard). The platform can then be used to plot the accelerations and calculate the ground-motion parameters for the event. The raw data are first run through a 0.1 Hz, high-pass, 4th order, Butterworth filter. The maximum amplitude for the peak ground acceleration (PGA) is then determined for the vertical component and the geometric mean of the horizontal components. The filtered acceleration data are integrated to velocities, which are then further integrated to displacements. The peak ground velocity (PGV) and peak ground displacement (PGD) are then determined for the vertical component and the geometric mean of the horizontal components. Additionally, the spectral intensity (SI), which provides a measure of the damage potential to structures by events, is calculated according to Rosenberger (unpublished report, 2010). The study defines SI as the maximum velocity of two, 20% dampened, single-degree-of-freedom systems with resonant frequencies of 1.5 s and 2.5 s. An example of an event recorded by one of the stations, displayed on the dashboard, is shown in Figure 1. Additional algorithms are currently being developed for real-time calculation of magnitudes, hypocentres and shake maps.

A simple amplitude threshold is being used for event detection. More sophisticated autodetection techniques were investigated (for a summary, see Li et al., 2018); however, the heavy contamination of the recordings at all stations from large-amplitude animal and anthropogenic noise makes auto-discrimination of seismic events difficult. In particular, seismic events recorded on single stations are difficult to discriminate from noise when the amplitudes are close to the digital noise (0.2 cm/s^2 for geometric mean of the horizontal components and 0.4 cm/s^2 for the vertical component). During dense deployments, a stacked local similarity function will be used for real-time discrimination of seismic events to ensure detection of smaller events.

Dataset

During the past year, the accelerographs were deployed to monitor two disposal wells, one in an active area of induced seismicity, and four hydraulic-fracturing completions, three of which were in an active area of induced seismicity. While a four-station array was deployed to monitor the disposal in the active area, single-station deployments were used to monitor the other operations. In addition to sites obtained through operator agreements, stations are also currently deployed at research sites and on a private ranch.

Although no events have yet been detected after 1.5 years by the station installed to monitor the disposal in a seismically inactive area, 12 events were recorded by the four-station array during its 6 months of operation. One event was recorded on three stations and three events were recorded on two stations. The event recorded by three stations in the array was the largest magnitude event reported by Natural Resources Canada (NRCan) from the Canadian National Seismograph Network (CNSN) stations during the deployment. The three events detected on two stations and five events detected by single stations were not reported by NRCan, while three other events detected by single stations were reported by NRCan. Two events reported by NRCan were missed by the four-station array (discussed further in the 'Magnitude of Completeness' section). All events recorded by both the study's array and the NRCan network have magnitudes between 2 and 3, and hypocentral distances between 10 and 14 km.

No events were detected during the first hydraulic-fracturing operation monitored this year, which was the smallest of the three operations in the seismically active area. The station was deployed for two months following the completions, in which time eight events with Mw > 1.5 were recorded on the local, operator-deployed (local) array in the area. The two largest events were recorded by the study's station, the largest of which was also reported by NRCan. During pre-completion monitoring, the two events were also detected by the station that was deployed for the second operation. Five out of the six Mw > 1.5 events and one event with Mw < 1.5 recorded by the local array during the second completion were detected by the study's station. One of the five events with Mw > 1.5 recorded on the local array during the third operation was not detectable above the digital noise.

In total, 25 events were recorded during the deployments, with pre–site-corrected PGAs (for geometric mean of horizontal components) ranging from 0.035%g to 0.29%g. Examples of typical 3-axis acceleration data for events recorded by the study's stations are shown in Figure 2.

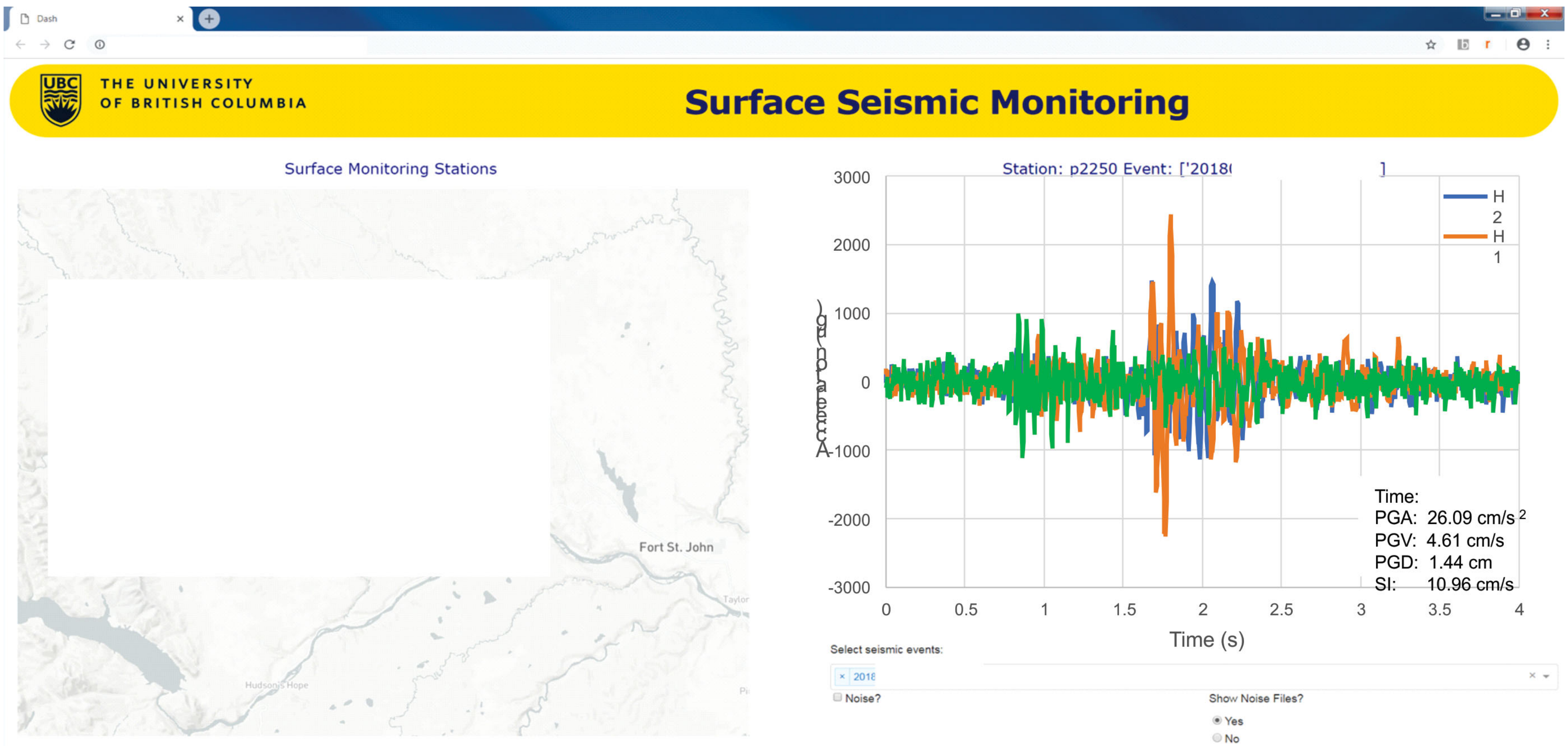

Figure 1. Example of typical 3-axis acceleration data recorded for a seismic event by one of the study's stations, as displayed on the online, interactive dashboard. Event time and station location have been removed for confidentiality.

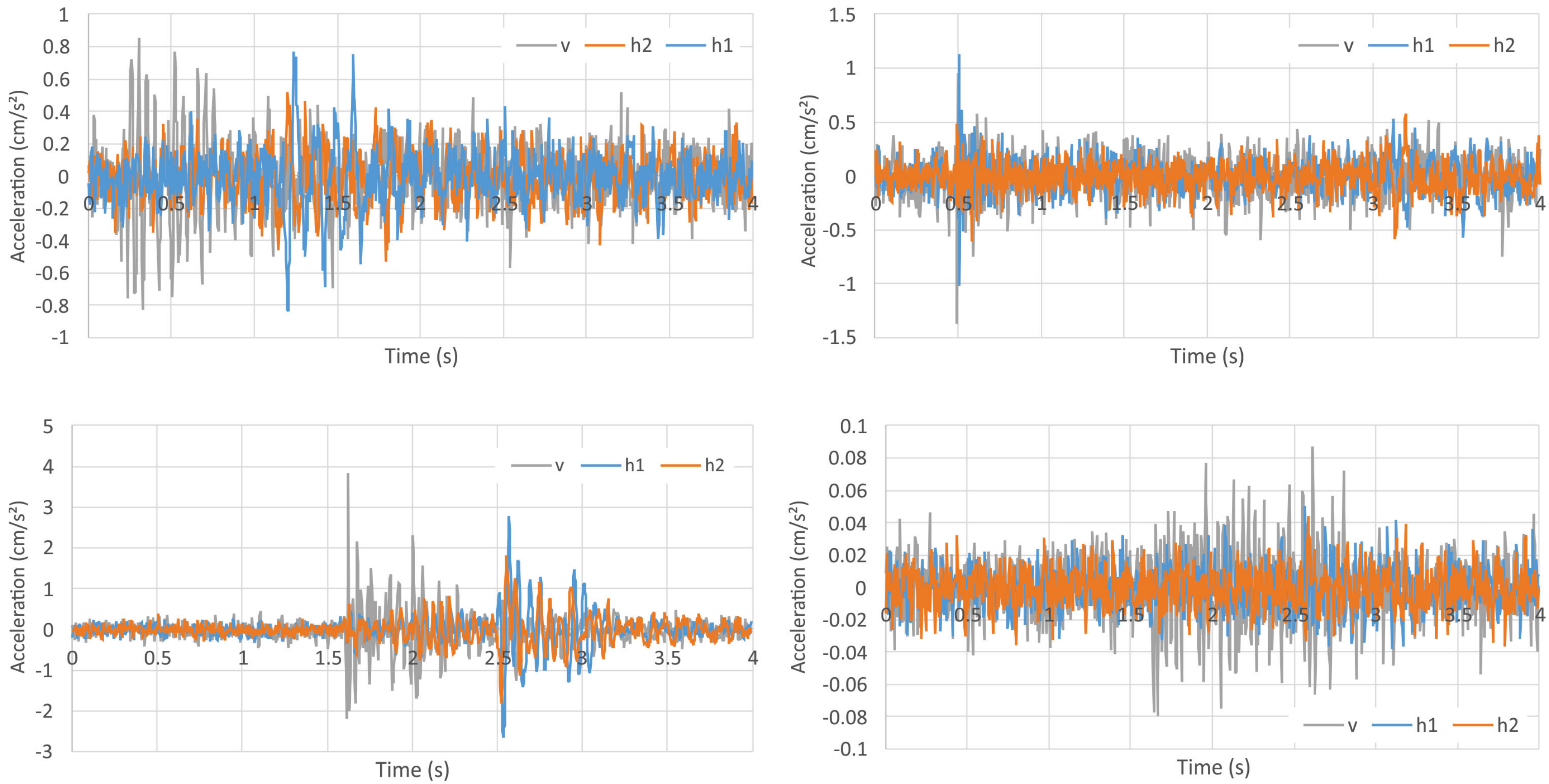

Figure 2. Examples of 3-axis acceleration data recorded for seismic events by the study's stations.

Site Corrections

The measured PGAs were corrected for each event to a reference site-class with a time-averaged shear-wave velocity over the top 30 m (V_{s30}) of 760 m/s using the amplification factors from Seyhan and Stewart (2014). In the first step, the response spectral acceleration (PSA) was calculated at frequencies of 0.1–100 Hz for the geometric mean of the horizontal components and the vertical component. The spectral ratio of the horizontal to vertical components (H/V) was then calculated for each event, following which the H/V ratios were log-averaged for each station. The H/V spectral ratios calculated for the study's stations are shown in Figure 3. The fundamental frequency (f_{peak}) was then defined as the frequency at the peak H/V amplitude. Using the correlation of Hassani and Atkinson (2016), V_{s30} values were estimated from f_{peak} for each station with recorded events. The class for each site could then be determined from V_{s30} based on the classification of the National Earthquake Hazards Reduction Program (NEHRP), which could then be used to determine the PGA correction factor (F_{PGA}). The V_{s30}, f_{peak}, site class and F_{PGA} for the study's stations are shown in Table 1. Following correction, the PGAs for the 25 recorded events range from 0.027%g to 0.23%g. The corrected PGAs, as well as the event magnitude and hypocentral distance when available, are shown in Table 2.

Attenuation

The site-corrected PGAs versus hypocentral distances for seismic events recorded by the study's stations were overlain on the data and predictive models presented for the Montney Formation by Babaie Mahani and Kao (2017). The results, which are plotted in Figure 4, show that the datasets are consistent; however, the predictive model for area (a) slightly underestimates the study's data.

Magnitude of Completeness

To investigate the magnitude of completeness for the sensors, the magnitude was plotted versus hypocentral distance in Figure 5 for events that were detected by one or more of the study's stations (blue) and events that were not detected (red). The results indicate that M > 1.5 events are consistently detected within 5 km and M > 2 events within 10 km of one of the stations. It is not possible to comment on the detection threshold for events with M < 1.5 because many smaller events are currently being missed by the simple amplitude threshold and single-station deployments. Three events stand out on Figure 5: one M ≈ 1.5 event with hypocentral distance of <1 km and two M ≈ 2 events at distances of ~5 km. A denser array would have been required to discriminate the cause of the lower-than-expected ground motions recorded for these events. A possible explanation is that the source radiated asymmetrically with a minimum axis in the direction of the study's stations.

Table 1. Values of V_{s30}, f_{peak}, site class and F_{PGA} for the study's stations with recorded seismic events.

Station	f_{peak} (Hz)	V_{s30} (m/s)	Class	F_{PGA}
1	8	587.42	C	1.3
2	10	676.08	C	1.3
3	8.33	602.57	C	1.3
4	10.5	697.19	C	1.3
5	18.2	985.93	B	0.9
6	7.7	573.44	C	1.3

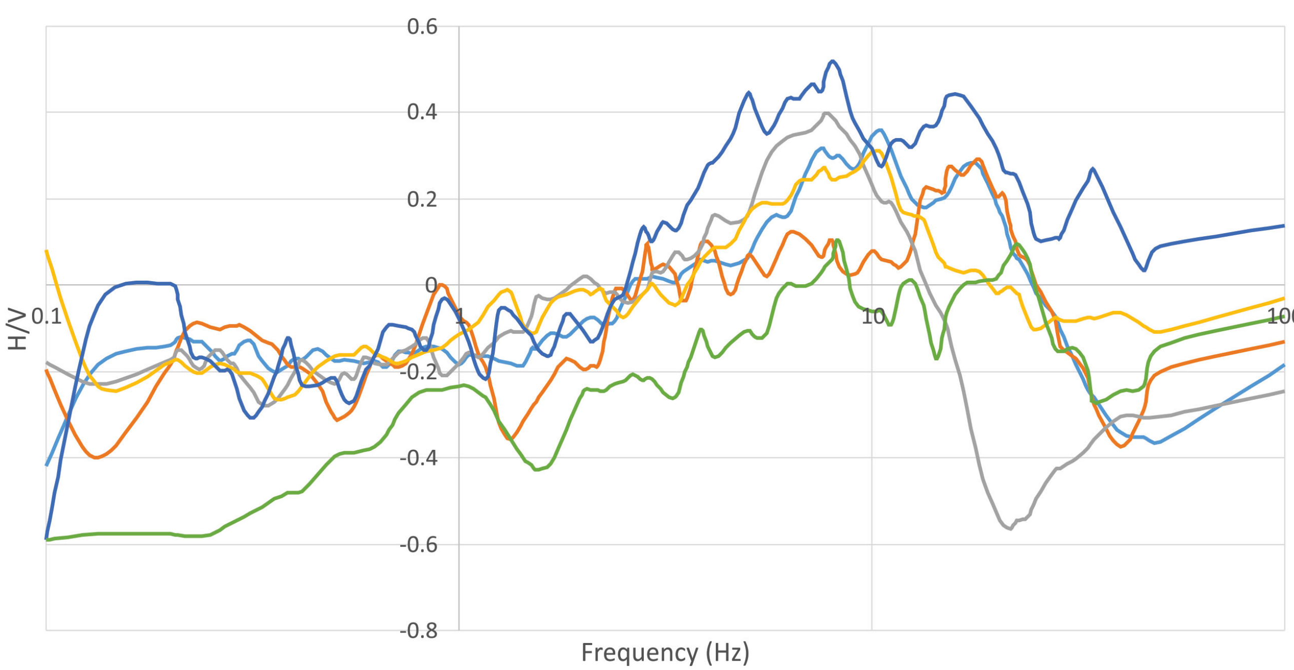

Figure 3. Log-averaged spectral ratio of horizontal to vertical components (H/V) versus frequency for each of the study's stations with recorded seismic events.

Table 2. Site-corrected PGA for each seismic event recorded by the study's stations, as well as event magnitude and hypocentral distance when available.

Event	PGAh (cm/s^2)	Distance (km)	M
1	0.48	5.9	1.8
2	0.27	5	1.64
3	0.55	2.2	1.77
4	0.68	1.2	1.74
5	2.22	9.1	2.88
	0.31	17.5	
6	0.27	13.3	2.5
7	0.27	12.6	2.3
8	0.35	12.2	2.5
9	1.54	11	2.7
	0.55	10.4	
	0.76	10.4	
10	0.3	4.6	1.74
11	0.52	5.9	1.54
12	0.31	4.6	1.62
13	0.46	5.1	1.88
14	0.33	6.4	1.72
15	0.36	5.6	1.57
16	0.54	4.9	2.23
17	0.96	4.5	
18	2.01		
	0.79		
19	0.57		
20	0.64		
21	0.97		
22	0.45		
23	0.76		
	1.44		
24	0.28		
	0.93		
25	1.07		

Depth of Burial

To investigate any possible effects that depth of burial of the study's sensors might have on recorded ground motions, four sensors were installed very recently at different depths (30, 60, 90 and 120 cm) at a single site in a seismically active area. The 90 cm station is the new paired station, while the 60 cm station is a long-term station already located at the site. The sensors are a maximum of 5 m apart, with the 30 and 90 cm sensors and the 60 and 120 cm sensors being within 1 m of each other. While waiting for an event, a test was performed in which a steel I-beam was struck several times with a sledgehammer at a distance of ~15 m from the stations. Due to the short distance between the tests and the stations, the difference in amplitudes (presented in Table 3 for a typical test) results from the varying source-receiver distance and not the depth of burial.

Summary

The study's accelerographs, which are now providing real-time data to an online interactive dashboard, were deployed to monitor two disposal wells and four hydraulic-fracturing operations in the past year. Twenty-five events were recorded during the deployments, with site-corrected PGAs for the geometric mean of the horizontal components ranging from 0.027%g to 0.23%g. These values are consistent with the data and prediction models previously presented for the Montney Formation. The study's first paired station with both a 3C accelerometer and a 3C geophone was recently deployed for testing, and algorithms are being developed for use with the dashboard to locate events and calculate magnitudes in real time. Additional ongoing work includes a study testing the impact of sensor burial depth on recorded ground motions.

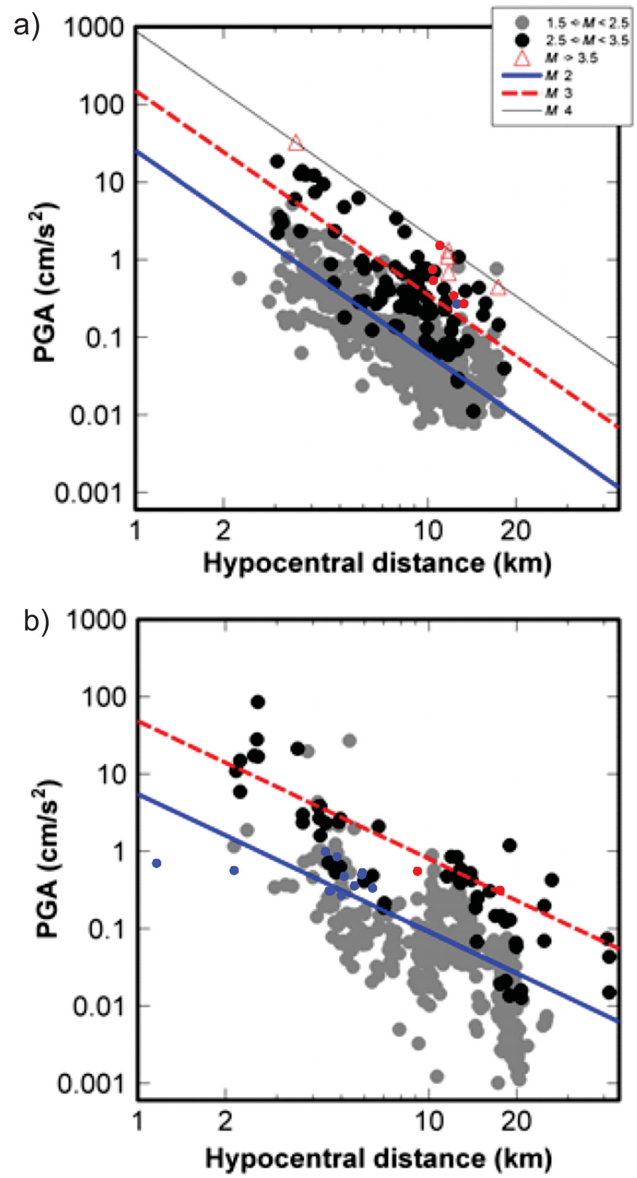

Figure 4. Site-corrected PGA versus hypocentral distance for seismic events recorded by the study's array, with events of 2.5 < M < 3.5 plotted as red dots **(a)** and those of 1.5 < M < 2.5 plotted as blue dots **(b)** on figures from Babaie Mahani and Kao (2017).

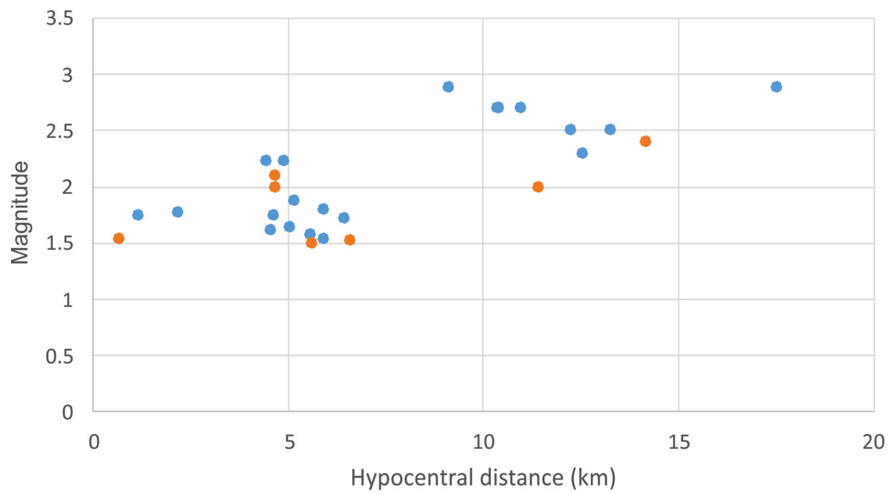

Figure 5. Magnitude versus hypocentral distance for events that were detected by one or more of the study's stations (blue) and events that were not detected (red).

Table 3. Comparison of PGA (PGAh, geometric mean of horizontal components; PGV, vertical component) from a typical I-beam test for the four stations co-located with different depths of burial.

Depth (cm)	PGAh (cm/s^2)	PGAv (cm/s^2)
30	18.05	22.84
60	32.21	42.51
90	27.48	41.83
120	10.24	17.23

Acknowledgments

The authors thank Geoscience BC for their support and funding for this study. Thanks also go to K. Johansen and C. Ventura for their help with the design and construction of the sensors, and R.M. Bustin for his review of this manuscript.

References

Azpiri, J. (2016): Early-warning system successfully detects B.C. earthquake; Global News, URL <http://globalnews.ca/news/2429129/early-warning-system-successfully-detects-b-c-earthquake/> [December 2018].

Babaie Mahani, A. and Kao, H. (2017). Ground motion from M1.5 to 3.8 induced earthquakes at hypocentral distance <45 km in the Montney play of northeast British Columbia, Canada; Seismological Research Letters, v. 89, no. 1, p. 22–34, URL <https://doi.org/10.1785/0220170119> [November 2018].

Bustin, A.M.M. and Longobardi, M. (2017). Collecting ground-motion data for the mitigation and prevention of seismicity induced by hydraulic fracturing in the Montney Formation, northeastern British Columbia; *in* Geoscience BC Summary of Activities 2017: Energy, Geoscience BC, Report 2018-4, p. 23–28, URL <http://cdn.geosciencebc.com/pdf/SummaryofActivities2017/Energy/SoA 2017_E_Bustin.pdf> [November 2018].

Hassani, B. and Atkinson G.M. (2016). Applicability of the site fundamental frequency as a VS30 proxy for central and eastern North America; Bulletin of Seismological Society of America, v. 106, no. 2, p. 653–664, URL <https://doi.org/10.1785/0120150259> [November 2018].

Li, Z., Peng, Z., Hollis, D., Zhu, L. and McClellan, J. (2018). High-resolution seismic event detection using local similarity for large-N arrays; Scientific Reports, v. 8, article 1646, URL <https://doi.org/10.1038/s41598-018-19728-w> [November 2018].

Seyhan, E. and Stewart, J.P. (2014). Semi-empirical nonlinear site amplification from NGA-West2 data and simulations; Earthquake Spectra, v. 30, no. 3, p. 1241–1256, URL <https://doi.org/10.1193/063013EQS181M> [November 2018].